

ABSTRACT

Within the frame of LAWENDEL project the laser weldability of Al-Li alloys AA2198 and AA2196 was studied to determine the process parameters needed to obtain consistent laser welds, and to compare the mechanical behaviour with the conventional fuselage aluminium alloy combination AA2024 and AA7075. To optimise the dual laser welding process for skin-stringer structures, a comprehensive finite element model was established based on ABAQUS and Finite Element Analysis Toolbox using the Welding Modelling Toolbox module. The model is able to predict the thermal history and size of fusion zone for various welding conditions and also able to expand to more complicated welding configuration. The microstructures of the welds were investigated and the strength loss in the heat affected zone was also characterised. A noticeable equiaxed grain zone was found in all welding conditions which impose reliability risk. Porosities and microcracks were also spotted inside the fusion zone and, even along the fusion boundary when the laser power reached 2000 W. A hot cracking susceptibility modelling was carried out on the basis of the composition characterisation. The study also emphasizes the mechanical properties of the weld joint to gain an understanding of the underlying factors controlling the performance of the welds. During the demonstration phase the developed laser beam welding technology was applied for welding stiffened flat panels. It was found that the fatigue strength of laser beam welded T-joints is approximately 23 % higher than that of riveted joint. The mechanical performance of the welded panels was investigated through the compression test.

1 INTRODUCTION

To meet the future demands of the aerospace industry with respect to safety, productivity, weight and cost, new materials and joining concepts have been developed. The platform Green Regional Aircraft of the European Clean Sky Programme has set the objective to investigate lightweight metal components for lighter aircraft structures. One objective of Clean Sky ITD (Integrated Technology Demonstrator) Eco Design is to investigate new joining technologies for new aluminium alloys. The scope of this approach is to develop lighter aircraft structures. Fuel saving and environmental advantages can be achieved through lighter airframe structures. Laser beam welding (LBW) as an efficient joining technology for fuselage structures is already established in the aircraft industry for lower fuselage panels, because the welded panels provide a higher buckling strength and lower weight compared with the classical riveted designs [1,2].

The recently developed Li-bearing aluminium alloys AA2198 and AA2196 are very promising high strength and lightweight alloys for aircraft manufacturing, for example, the skin-stringer T- joints for fuselage panels [1,3]. The modern aircraft manufacturing has adopted the LBW of skin-stringer structures due to the weight savings advantage by replacing the traditional riveted differential structure by an integral welded component [4]. However, Li-bearing aluminium alloys typically present severe weldability issues including high hot cracking sensitivity, formation of porosity and degradation of the mechanical properties of the joints [1,3].

The objective of the Eco-Design ITD project LAWENDEL accomplished within European Clean Sky Programme was to study the laser weldability of Al-Li alloys AA2198 and AA2196, to determine the process parameters needed to obtain consistent laser welds, and to compare the mechanical behaviour with the conventional aluminium alloys series. The study emphasizes the microstructure characteristics and the mechanical properties of the weld joint to gain an understanding of the underlying factors controlling the performance of the welds. During the demonstration phase of the project, the developed LBW technology was applied for welding stiffened flat panels in order to evaluate the industrial application. The mechanical performance of the welded panels was investigated through the compression tests. The innovative combination of state of the art modelling and experiments enabled physics based optimization of the welding process with greatly reduced time and cost compared to traditional trial and error methods.

2 EXPERIMENTAL

2.1 Materials

The materials for welding were supplied by Constellium and the detailed chemical composition is listed in **Table 1**. The base material (BM) AA2196 used for welding was fabricated by extrusion while the AA2198 was fabricated by rolling. Both alloys were in T8 temper. The AA2198 BM with a lower strength and higher ductility was used as the skin in order to fulfil the requirement of higher strength of the stringer material (AA2196). The materials properties used for LBW process simulation were also provided by Constellium [5]. The thermal conductivity and specific heat are temperature-dependant and latent heat due to the solid-liquid phase transformation is considered in the model. It is assumed the materials are continues and there is no materials loss during the LBW process.

Table 1: Chemical composition (wt.-%) of the three aluminium alloys.

Material	Si	Fe	Cu	Mn	Mg	Cr	Zn	Ti	Ag	Li	Zr	Al
AA2198	0.03	0.05	3.33	0.03	0.32	0.05	0.02	0.02	0.27	0.98	0.14	Bal.
AA2196	0.03	0.06	2.88	0.32	0.34	0.01	0.02	0.02	-	1.7	0.11	Bal.
AA4047	12.0	0.8	0.3	0.15	0.1	-	0.2	-	-	-	-	Bal.

2.2 Laser Beam Welding

The prototype of skin-stringer T-shaped welding joint comprises three materials, AA2198 as the skin, AA2196 as the stringer and AA4047 as the filler. As shown in **Figure 1**, the 3.2 mm thick skin sheet is vacuum clamped on an aluminium base while the extruded profile stringer is placed vertically on the skin sheet. The presence of lithium in the alloys increases the growth rate of the oxide film on the surface, which is mainly responsible for the formation of porosity during the welding. Therefore, extra attention needs to be paid to prepare the surface before welding. The surface of the skin material was grinded with sand paper to remove the oxide layer. It was found that the oxide layer on AA2196 contains a high hydrogen level, so the surface of the stringer AA2196 was milled down at least 0.2 mm. The final thickness of stringer after surface preparation was 1.6 mm. AA4047 filler wire with a diameter of 0.8 mm was used because its high percentage of Si can reduce the hot cracking. Two CO₂ laser beams were applied simultaneously on both sides of the stringer at a fixed incident angle of 22°. The filler wire and helium shielding gas were supplied in front of the laser beam on both sides of the stringer as well. The focal position of the laser beam was 0.0 mm on the stringer surface and +0.2 mm above the skin. The beam diameter was 250 µm with the focus length of 150 mm. Three welding experiments at laser power of 1400 W, 1720 W and 2000 W were carried out for calibration of FE-models. During the LBW experiments the transient temperature fields were measured by thermocouples. The optimized LBW parameters with regard to the microstructure and mechanical properties of welds were used for welding of the demonstrator panel with four stringers (**Figure 13(a)**).

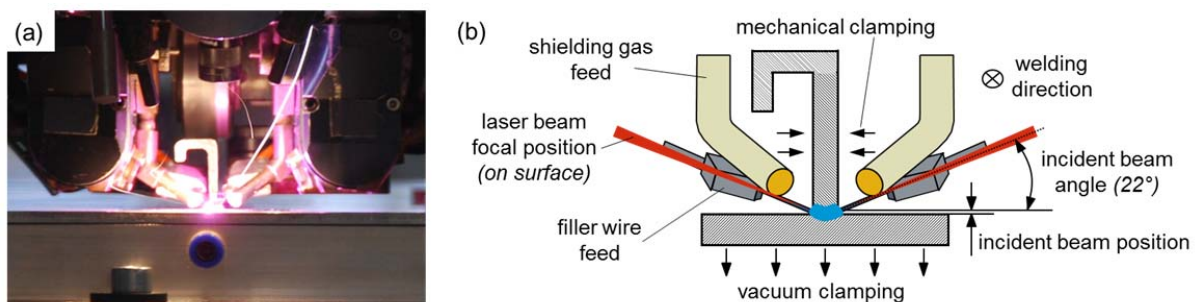


Figure 1: (a) Photo of a laser sequence and (b) configuration of the laser welding skin-stringer process [3].

2.3 Laser Beam Welding Process Simulation

ABAQUS was used as a general modelling tool in this study. In order to model multiple moving heat sources directly in ABAQUS, a complex FORTRAN subroutine was required. Another FE-analysis software, namely the Finite Element Analysis Toolbox (FEAT), was utilised to define the heat source and applied into the model. It has a designated powerful Welding Modelling Toolbox (WMT) to perform accurate welding thermal and stress/strain modelling. By combining the advantages of ABAQUS and FEAT-WMT, a new modelling process has been developed which is illustrated in **Figure 2**.

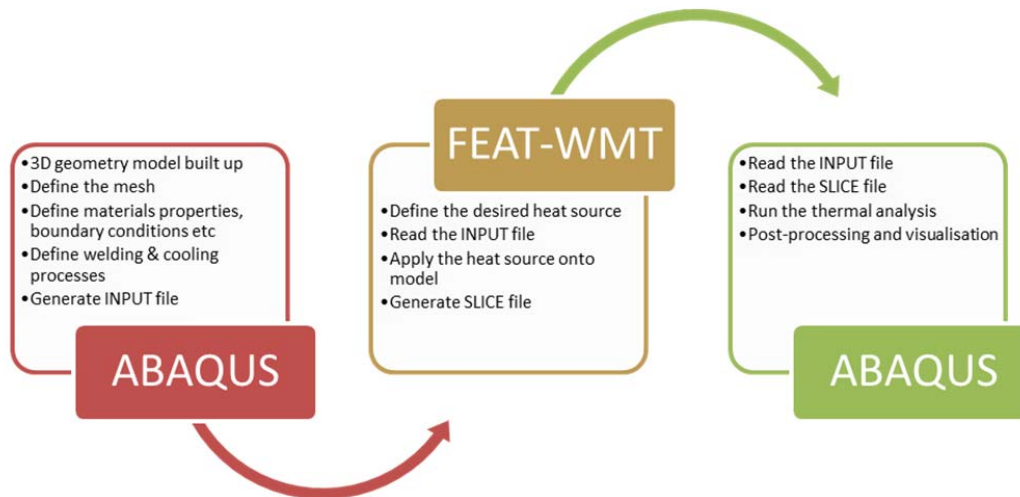


Figure 2: LBW process simulation by combining ABAQUS and FEAT-WMT.

In the new modelling process, the geometry model was firstly created in ABAQUS. Then, the materials properties, boundary conditions, meshing, welding process and cooling time are defined as well. The only item absent in this stage is the heat source. An INPUT file containing complete information of the model was thereafter generated. As designed, FEAT-WMT can read the ABAQUS INPUT file smoothly. The heat source was defined in FEAT-WMT by using the comprehensive templates and applied into the 3D model read from ABAQUS. FEAT-WMT then generated a series of SLICE files which contain the information of the moving heat source. Next, the INPUT file and SLICE files generated from the previous steps were read into ABAQUS again. The SLICE files were organised by a simple FORTRAN subroutine and were able to make up the moving heat source in ABAQUS without error. The thermal analysis was then carried out in ABAQUS using the standard solver.

An elliptic cone heat source is adopted in this study which is derived from the classic Goldak double ellipsoid and conical models [6][7]. As shown in Figure 3, the front part of the double elliptic cone is defined as:

$$q_f(x, y, z) = \frac{6f_r Q}{abc_f \pi(1+d_c)} \exp\left(-3\frac{x^2}{a^2}\right) \left[1 - \frac{(1-d_c)|y|}{b}\right] \exp\left(-3\frac{z^2}{c_f^2}\right) \quad (1)$$

and the rear part as:

$$q_r(x, y, z) = \frac{6f_r Q}{abc_r \pi(1+d_c)} \exp\left(-3\frac{x^2}{a^2}\right) \left[1 - \frac{(1-d_c)|y|}{b}\right] \exp\left(-3\frac{z^2}{c_r^2}\right) \quad (2)$$

where Q is the energy input, a , b and c are the geometric features of the double ellipsoidal and conical heat sources. The parameter d_c is a normalised parameter and has a value between 1 and 0. It is to define the percentage of energy intensity decreases through the depth. If the d_c is set as 1, that means

the energy intensity is constant from the top to the bottom of the cone, while $d_c = 0$ means the energy intensity decreases to zero at the bottom of the cone. The parameters f_f and f_r are the fractions between the front and rear parts in the conical functions respectively. To keep continuity between the front and rear parts of the combined heat source, they should satisfy the following relationships:

$$\begin{cases} f_f = \frac{2c_f}{c_f+c_r} \\ f_f + f_r = 2 \end{cases} \quad (3)$$

By varying the value of a , b and c , it allows one to quickly simulate the LBW process with various size of keyhole and different penetration depth.

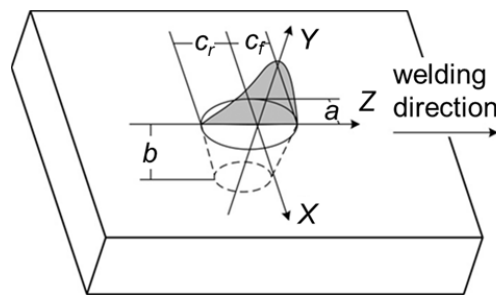


Figure 3: Configuration of the elliptic cone heat source.

The weld seam length is 310 mm corresponding for 3 seconds welding time (**Figure 4(a)**). However, because the welding becomes quasi-steady status soon after starting point, it is reasonable to reduce the length of the weld to 100 mm. The actual 3D model is shown in **Figure 4(b)**.

Based on the welding conditions and modelling procedure described above, the thermal modelling was conducted by combining ABAQUS 6.13 and FEAT-WMT. **Figure 4(c)** shows an example of the temperature field of the quasi-steady LBW process. It can be seen that the model successfully applied both heat sources onto the structure simultaneously, as expected. To validate the modelling results, a series of thermocouple data was obtained to be compared with the simulated values.

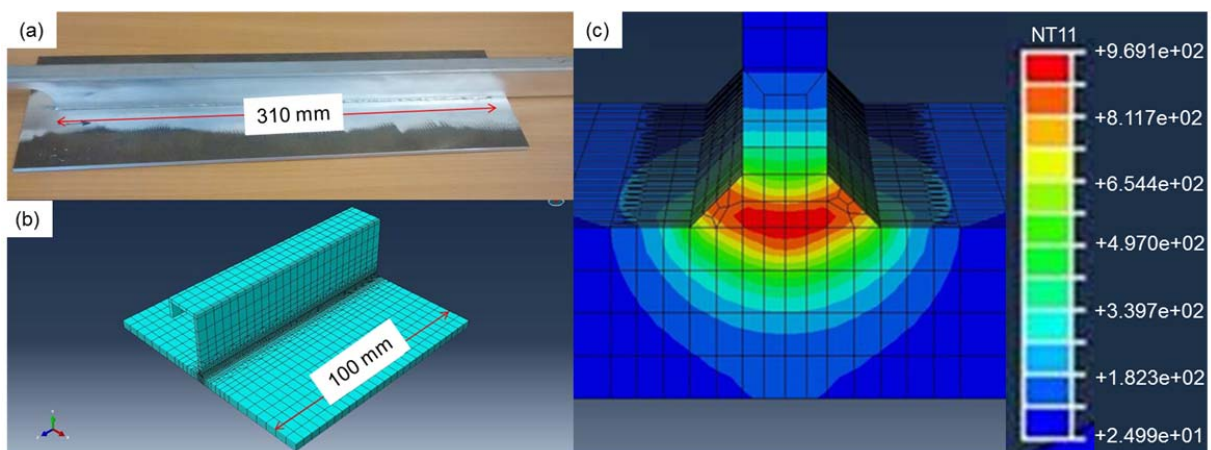


Figure 4: (a) The laser beam welded specimen, (b) the 3D FE-model built in ABAQUS and (c) an example contour map of the temperature field during the quasi-steady LBW process.

2.4 Microstructural and Mechanical Characterization

The microstructures and the phase formation of the welds were analysed by optical microscopy. Therefore the microsections of the welds were grinded, polished and then etched with Keller's reagent. Selected welds were investigated by the use of the scanning electron microscope (SEM) on polished microsections.

The static tests were performed in an electromechanical universal-testing machine (SchenckTrebel RM100), except for the tensile test of the riveted specimen. Due to the specimen size and resulting clamping necessities a servo-hydraulic testing machine (Schenck 1000 kN) was used. Fatigue tests of the riveted specimens were performed in a servo-hydraulic testing machine (Schenck 400 kN); the laser beam welded specimens were tested in a magnet-resonant machine (Russenberger Testronic 100 kN). The riveted specimens were delivered ready-to-test by Hellenic Aerospace Industry S.A., with a cross section of 400 mm², sheet thickness 2 mm, width 200 mm, 10 rivets (**Figure 5(a)**). The geometry of the laser beam welded specimens for fatigue testing was based on standard EN DIN 6072, cross section 65 mm². The specimens for static loading tests were manufactured according to ISO EN DIN 6892 (**Figure 5(b)**).

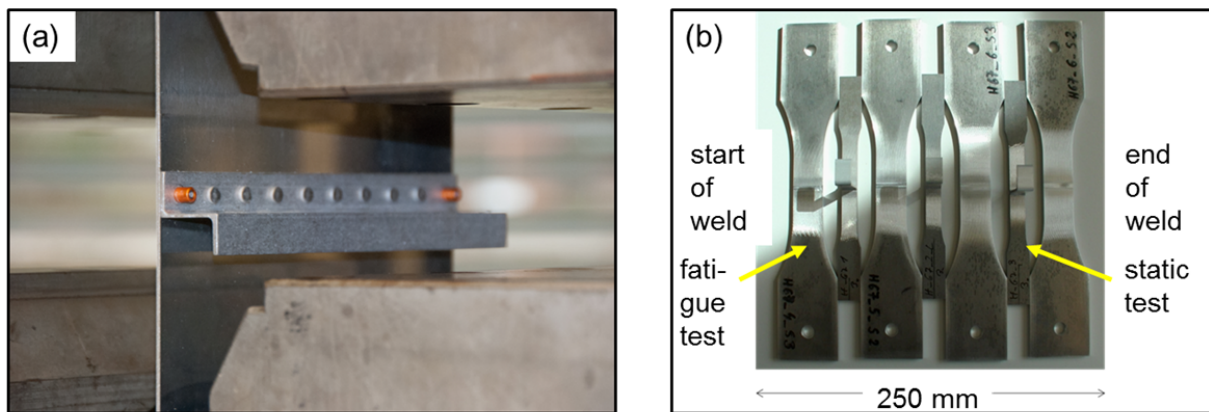


Figure 5: (a) Riveted specimen for static loading in the testing machine and (b) hoop-stress specimens for static loading and fatigue tests from laser beam welded panel.

In order to complete the mechanical characterization of LBW a compression test of a laser beam welded demonstrator was accomplished. The demonstrator panel with four laser beam welded stringers had a size of 384 mm x 736 mm. In **Figure 11(a)** the mounted demonstrator is shown. It was decided to fix the upper and lower end of the specimen in a clamping device, to prevent movements of the stringer and the skin caused by buckling. The test was performed with a displacement of 0.5 mm/min. Load and displacement were recorded with a standard data acquisition system.

3 RESULTS AND DISCUSSION

3.1 Laser Beam Welding Process Optimization

The LBW process development was accomplished by a combination of modelling and experiments. For this purpose the modelling approach described in section 2.3 for the prediction of the weldability and the mechanical properties after welding on basis of the process parameters and initial material properties was developed. This model was calibrated on basis of welding experiments for selected cases. After the experimental calibration the developed models were used for the numerically based optimization of the welding process with the goal to identify an optimum process window for reaching the best balance between good weldability and high mechanical properties after welding.

Figure 6 shows the comparison of the fusion boundaries between the simulation and experiments with different laser powers. With the increase in laser power, the fused area increases correspondingly. In this model, the volume of the filler material is calculated according to the diameter of the wire and the feeding rate, and then a pre-defined filler material area is fixed. Therefore, the profile of the weld bead in the model may not match the actual sample, but the width of the melted area and depth melting into both skin and stringer agree very well with experiments. This can be seen as a validation of the accuracy of the model.

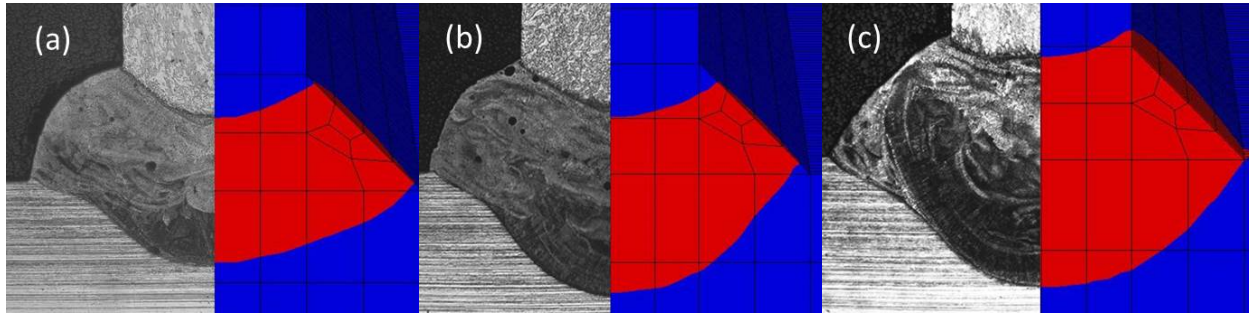


Figure 6: Comparison of the fusion zone dimensions between simulation and experiments with various laser powers: (a) 1400 W; (b) 1720 W; and (c) 2000 W.

The Al-Cu-Li alloys suffer from severe hot cracking problems [1,3,9,10], as revealed in the microstructures below (**Figure 8(b)**). It is of great interest to understand to what extent the hot cracking will occur during welding and to predict the hot cracking susceptibility (HCS) from a material's point of view. A hot tearing criterion has been developed by Rappaz, Drezet and Gremaud on the basis of a mass balance over the liquid and solid phases during the solidification process [8], i.e. the so called RDG model. Great details of the model can be found in the reference. The hot cracking susceptibility is represented by an 'A' parameter which is defined as:

$$A = \int_{T_{coh}}^{T_l} \frac{f_s^2 \int_{T_{coh}}^T f_s dT}{(1-f_s)^3} dT \quad (7)$$

where T_{coh} is the coherency temperature that the weld contains 96% of solid phase, f_s is the solid fraction by volume which can be calculated by JMatPro using Scheil-Gulliver equation on the basis of the composition. With this model available, it is possible to predict the hot cracking susceptibility by knowing the detailed composition of the alloy.

As mentioned above, the fusion zone of the welds feature inhomogeneity of composition. It is possible to predict the HCS by using the RDG model and draw a relative hot cracking susceptibility map over the entire fusion zone. **Figure 7** plots the contour map of 'A' parameters calculated by the RDG model across the fusion zones of the welds made in 1400 W, 1720 W and 2000 W laser. The composition of the fusion zone was extracted from the EDX mapping. When the laser power is 1400 W (**Figure 7(a)**), the homogeneity of the fusion zone is in the worst situation so that the bottom of the weld has relatively high hot cracking susceptibility, i.e. larger 'A' value. When the laser power increases to 1720 W (**Figure 7(b)**), the mixing homogeneity of the three materials is improved and the centre of the fusion zone has relatively uniform hot cracking susceptibility. However, in this sample, perhaps less filler material was added to the right hand side fillet and that area tends to be more sensitive to hot tearing. In the case of LBW at 2000 W (**Figure 7(c)**), the fillet area shows higher hot cracking susceptibility than the middle of the fusion zone.

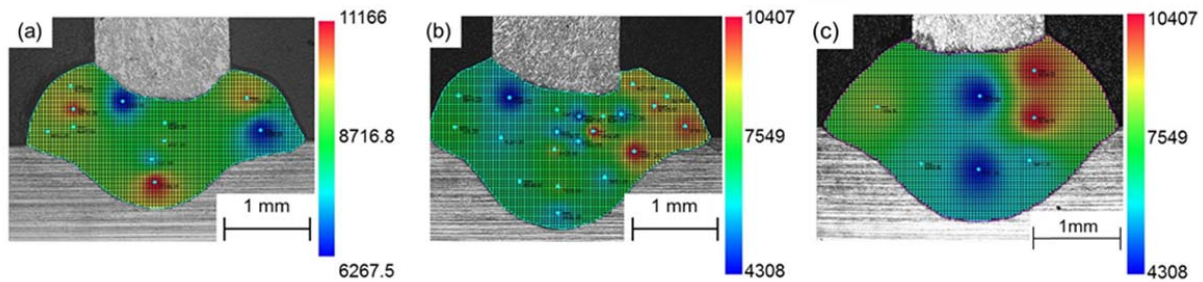


Figure 7: Contour maps of HCS 'A' parameter calculated by RDG model: (a) 1400 W laser power; (b) 1720 W laser power; (c) 2000 W laser power.

Figure 8 shows the microstructure of the weld made by 1400 W laser power. The grains in fusion zone are refined due to the relatively concentrated energy input and rapid cooling effect. In general, post-welding aging strengthening in the fusion zone is very limited because most of the solute needed to form the precipitates is locked in the eutectic constituent during the solidification process. Outside the fusion zone is the heat affected zone (HAZ) where the heat flows into the BM. Some of the precipitates in the HAZ zone are dissolved or coarsened by the heat flow resulting in strength loss which can be seen in the microhardness profile (**Figure 9(a)**). Unlike conventional arc welding, laser welding features a relatively small HAZ zone.

Adjacent to the fusion boundary within the fusion zone, a small area of fine equiaxed grains is observed in all welding conditions. The so-called equiaxed grain zone (EQZ) only occurs in Li-bearing aluminium alloys, as shown in **Figure 8(b)** and **(c)**. The width of the EQZ next to the AA2196 base material increases from the outside towards the centre of the weld **Figure 8(b)**. Next to the EQZ, the grains grow towards the centre of the weld following the gradient of the heat flow. In the area close to the fusion boundary, micro-cracks are found in transverse to the grain growth direction. The EQZ is associated with severe cracking problem during welding. It has been reported that cracks are often found in EQZ in Varestraint test [9]. In this study, severe cracks are found in the EQZ along the fusion boundary in the weld made with 2000 W laser. The formation of the EQZ can be explained by the recrystallization in the HAZ adjacent to the fusion zone or heterogeneous nucleation on the precipitates or dispersoids survived in the thermal cycle [10]. Some researches show that EQZ can be eliminated by using one of the following approaches: (1) stirring welding pool, (2) change material composition and (3) change the nature of the parent metal [9].

The formation of pores and cracks is a common challenge during LBW of Al-Li-alloys [1,3,9,10]. Based on the modelling and experimental results a good compromise was found in case of laser power of 1720 W, so it was decided to use this parameter set for further LBW experiments.

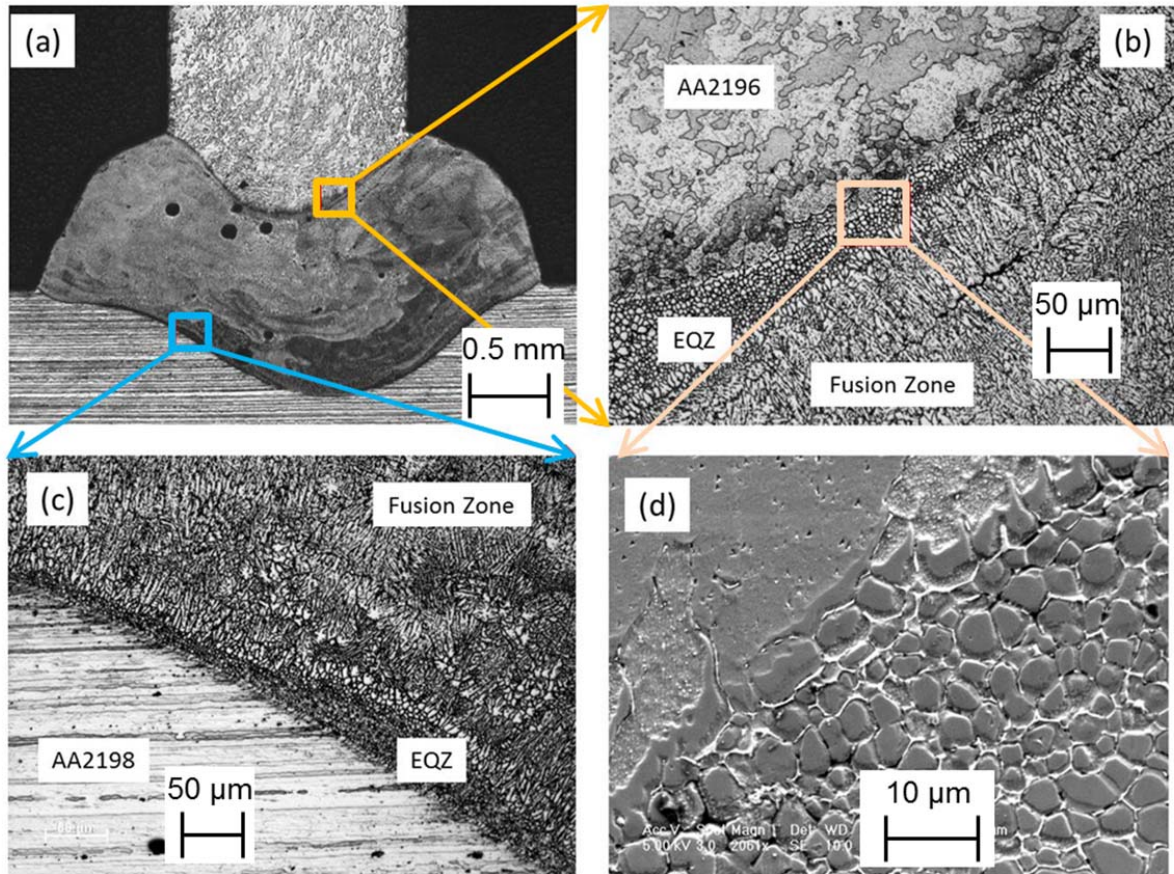


Figure 8: Microstructure in different areas of weld produced by 1400 W laser power: (a) overall view of weld; (b) fusion boundary on stringer; (c) fusion boundary on skin; (d) equiaxed grain zone.

In order to find out to what extent the weld joint is weakened, Vickers microhardness indentations were made across the weld's cross-section through two directions: through the height of the weld from stringer to skin (Y direction) and through the width of the weld across the skin only (X direction). **Figure 9(a)** depicts the HV 0.2 microhardness map of a specimen welded at a laser power of 1720 W. It can be seen that the fusion boundary has the lowest hardness which corresponds to the EQZ mentioned above. The microhardness in the grain boundary drops to about 60% of BM and recovers to about 75% of BM in the weld centre. The partial recovery of hardness in the centre of weld reflects to the casting structure which loses the precipitation hardening effects. The size of HAZs in AA2198 was calculated on the basis of the hardness change. When the laser power is 1400 W and 1720 W, the HAZ zone in the skin is about 0.8 mm wide in average. When the laser power increases to 2000 W, the HAZ zone slightly increases to about 1.0 mm outside fusion boundary. In order to compensate the weakening of the skin due to the LBW, the welding of the stringer is considered on a socket with the total thickness = thickness of the skin + the width of the HAZ (**Figure 9(b)**).

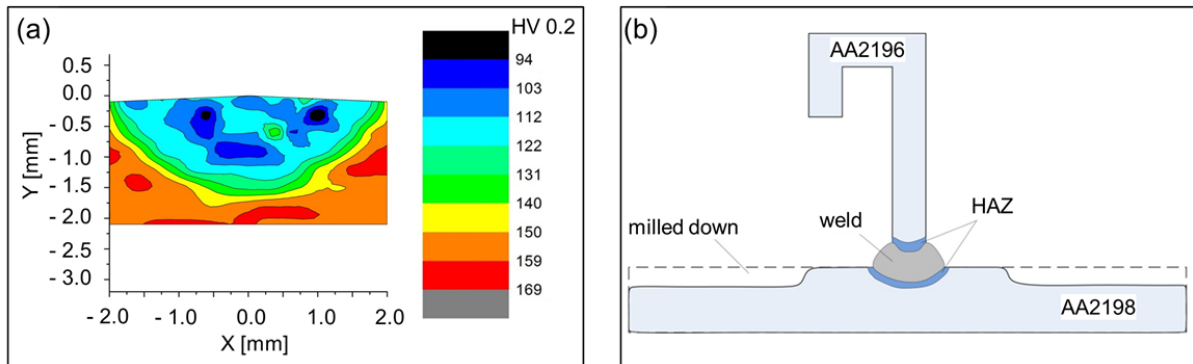


Figure 9: (a) Microhardness profile of the weld and (b) schematic configuration of welded coupon with material to be removed from skin fusion boundary on stringer.

3.2 Mechanical Properties of the Joints

Figure 10(a) shows the hoop-stress test results with the tensile test results of BMs. Due to softening under the weld, in case of the tensile specimen with T-joint the strain is localized in the softer regions leading to a limited strain to fracture. In different T-joints welded at a laser power of 1720 W different values for the yield strength (YS) and ultimate tensile strength (UTS) were determined. The characteristic values are given in **Table 2**, where YS is Rp0.2 for the BM. A joint efficiency of at least 76 % was received, with of over 80 %. The maximal loss of strength determined in the tested laser beam welded specimens was -24%, which will lead in direct comparison to a necessary socket under the weld of 0.8 mm (**Figure 9(b)**). It must be mentioned, that this value is only valid for 3.2 mm thickness of the sheet. If thinner sheets are welded, the heat distribution has to be taken into account, which may influence other thicknesses in a different way. The higher strength of the stringer plays no role in this loading case it is connected via a low strength zone. Just the geometry with the stringer perpendicular to the loading direction in the middle of the specimen may lead to strain concentration under the stringer. In **Figure 10(a)** a representative stress-strain curve of AA2024T3 BM is also shown. Base material is compared with the riveted joint. For the riveted joint the full area of 200 mm x 2 mm was considered. A joint efficiency of 64 % was reached (**Table 3**).

Table 2: Results of the tensile (BMs) and hoop-stress test (four panels laser beam welded at the same process parameter set (1720 W)).

Number	YS (MPa)	UTS (MPa)	A _{50mm} (%)	YS dev. (%)	UTS dev. (%)
AA2196T8 BM L-T	550	589	7.9	+14	+12
AA2198T8 BM L-T	481	528	11.3	0	0
LBW panel 1	420	435	0.70	-13	-18
LBW panel 2	368	408	0.78	-23	-23
LBW panel 3	370	400	0.81	-24	-24
LBW panel 4	411	435	0.77	-15	-18

Table 3: Results of the tensile (AA2024T3 BM) and hoop-stress test (riveted specimen).

Number	YS (MPa)	UTS (MPa)	A _{50mm} (%)	YS dev. (%)	UTS dev. (%)
AA2024T3	323	472	19	0	0
Riveted	298	300	11.3	-8	-36

Comparing riveted and laser beam welded specimens, **Figure 10(a)** highlights that the Al-Li alloys show a slightly higher elastic modulus – theoretically 1 % of Li shall increase it by 6 %. The strain to fracture of the laser beam welded joints is much larger than that of the riveted joint, but without the existence of Rp0.2 the joint is stiffer and more sensitive to strain. Theoretically, with static loading transverse to stringer, AA2198T8 skin must be 1.615 mm thick to bear the same load as 2.0 mm AA2024T3 skin. For 1 m² the weight saving would be 25 %, without taking the stringers into consideration and calculating with the following densities: AA2198 = 2.619 g/cm³ and AA2024 = 2.79 g/cm³.

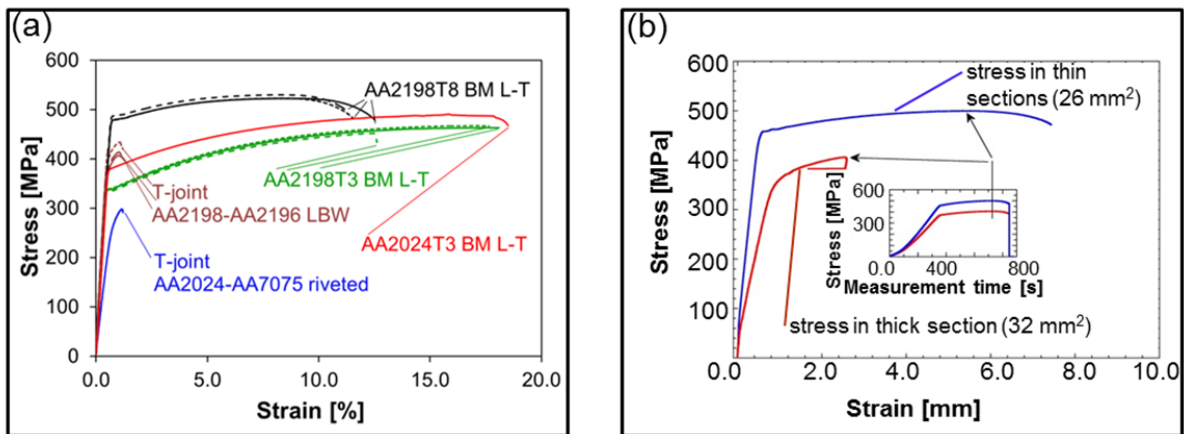


Figure 10: (a) Tensile test results (with hoop-stress test); (b) Stress-strain curve of laser beam welded AA2198-AA2196 T-joint with milled socket (**Figure 9(b)** and **Figure 11**).

For laser beam welded structures it is recommended, that the weld zone shall be reinforced by a socket as shown in **Figure 9(b)**. This socket will protect the weld area and the fracture should occur in the BM. The socket height was determined by comparing the fracture load of the hoop-stress test with the base materials tensile strength. This led to a difference in thicknesses of 0.7 mm. For testing this second set of hoop-stress specimens more detailed deformation analysis was done. As can be seen in **Figure 11(a)**, four white stripes were attached to the specimen. From this set-up it is possible to determine the global strain between the outer stripes and local strains between the different stripes. The data evaluation was limited to the inner (the socket area) and the global strain. Two of these curves are displayed in **Figure 10(b)**. The stresses were calculated according to the thickness of the section, the shielding effect of the socket is clearly visible. All of the four tested specimens broke in the thinned region of the BM (**Figure 11(b)**). It must be mentioned, that according to skin thickness and welding parameters, other sockets will be necessary.

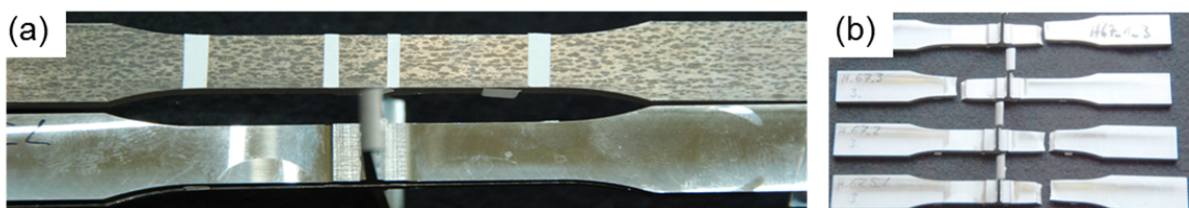


Figure 11: (a) Photo of two laser beam welded specimens with the socket geometry for the hoop-stress test: upper one is the skin side with stripes for the strain measurement with a laser extensometer, lower one is the stringer side;
 (b) Photography of the tested specimens with the socket geometry for shielding of the weld zone.

The fatigue strength of LBW AA2198/AA2196 was determined to be 80 MPa, 23 % higher than the strength of riveted AA2024/AA7075, which was 65 MPa (**Figure 12**). The laser beam welded joints suffer here from relatively sharp inconsistencies in the weld zone where cracks can initiate more easily, as in the riveted joints with relatively large smooth holes. Theoretically, with fatigue loading ($R=0.1$) transverse to stringer, AA2198T8 skin must be 1.625 mm thick to bear the same load as 2.0 mm AA2024T3 skin. For 1 m² the weight saving would be 25 %, without taking the stringers into consideration and calculating with the following densities: AA2198 = 2.619 g/cm³ and AA2024 = 2.79 g/cm³

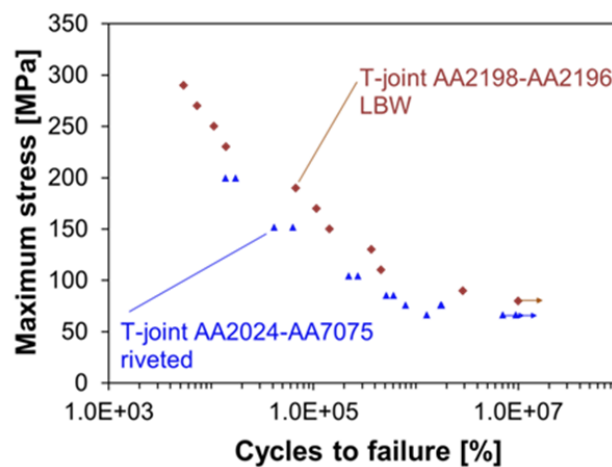


Figure 12: Fatigue test results.

3.3 Compression Test

The compression test of laser beam welded panel with four stringers was performed to complete the mechanical characterization. **Figure 13(a)** shows the welded demonstrator mounted for the compression test. **Figure 13(b)** shows the demonstrator after failure. The load-displacement curve is displayed in **Figure 13(c)**. It can be seen, that no plastic deformation occurred till fracture. The skin flipped to buckling and the stringers were separated by the fracture on their whole length. The demonstrator reached a load of 365 kN than skin buckled and stringers broke away on full length.

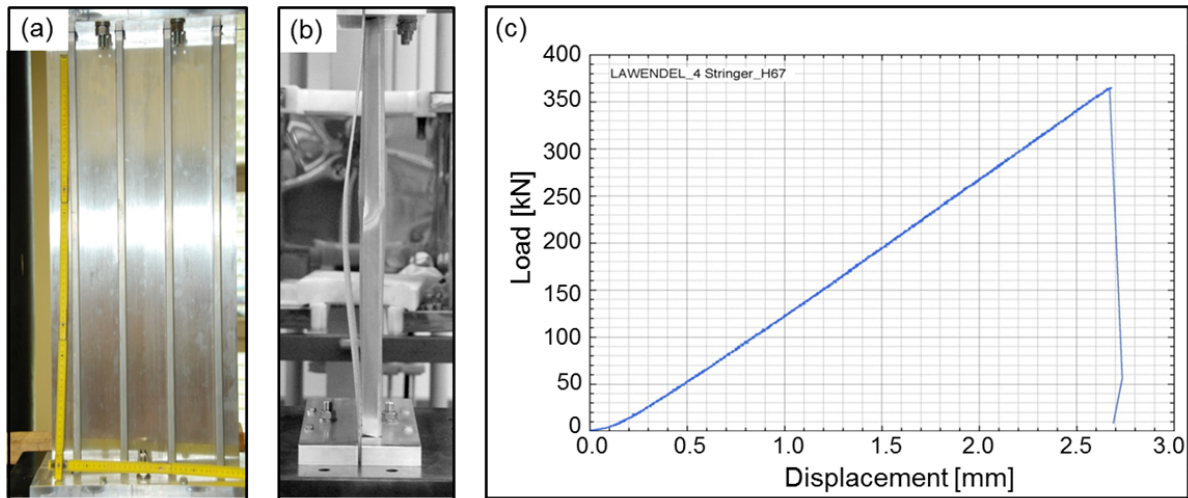


Figure 13: (a) Laser beam welded demonstrator mounted for the compression test, (b) the demonstrator after failure and (c) load vs. displacement curve of the compression test.

4 CONCLUSIONS

In summary, the following conclusions can be drawn from the accomplished research:

- A finite element process model has been successfully developed and validated with the experimental data;
- The model uses ABAQUS and FEAT-WMT and can predict the thermal history of any point in the welding process and the size of fusion zone under various welding parameters.
- The hot cracking susceptibility has been modelled by using RDG model and Scheil-Gulliver equation.
- According to the microstructure analysis, welds made with 2000W laser have most severe defects. It is suggested that to keep the laser power in a relatively lower level, e.g. 1400 W-1720 W.
- For the laser beam welded joints YS and UTS are minimum 76% of the AA2198T8 base materials;
- Compared to a riveted joint of AA2024/AA7075 YS and UTS of the welded AA2198/AA2196 joint are 25% higher;
- Fatigue strength of laser beam welded AA2198/AA2196 T-joint reaches 85 MPa; It is 23% higher than that of riveted AA2024-AA7075;
- Theoretically a weight saving of 25 % could be possible when using LBW of AA2198/AA2196 instead of riveting AA2024-AA7075;
- The demonstrator reached a load of 365 kN during the compression test, than skin buckled and stringers broke away on full length.

REFERENCES

- [1]. D. Dittrich et al.: Laser Beam Welding of Hard to Weld Al Alloys for a Regional Aircraft Fuselage Design – First Results. *Physics Procedia*. 2011; 12: pp. 113–122.
- [2]. B. Lenczowski: New Lightweight Alloys for Welded Aircraft Structure, International Council of the Aeronautical Sciences Congress, Toronto, 2012.
- [3]. J. Enz et al.: Influence of the Local Chemical Composition on the Mechanical Properties of Laser Beam Welded Al-Li Alloys. *Physics Procedia*. 2012; 39: pp. 51-58.
- [4]. M. Pacchione, J. Telgkamp: Challenges of the Metallic Fuselage, International Council of the Aeronautical Sciences Congress, Hamburg, 2006.
- [5]. www.constellium.com.
- [6]. A. Lundbäck and H. Runnemalm: Validation of three-dimensional finite element model for electron beam welding of Inconel 718. *Sci. Technol. Weld. Join.*, vol. 10, no. 6, pp. 717–724, Dec. 2005.
- [7]. J. Goldak et al.: A new finite element model for welding heat sources. *Metall. Trans. B*, vol. 15, no. 2, pp. 299–305, Jun. 1984.
- [8]. M. Rappaz et al.: A new hot-tearing criterion. *Metall. Mater. Trans. A*, vol. 30, no. 2, pp. 449–455, Feb. 1999.
- [9]. A. Kostrivas and J. C. Lippold: Weldability of Li-bearing Aluminium Alloys. *Int. Mater. Rev.*, vol. 44, no. 6, pp. 217–237, 1999.
- [10]. A. Gutierrez and J. C. Lippold: A proposed mechanism for equiaxed grain formation along the fusion boundary in aluminum-copper-lithium alloys. *Weld. J.*, vol. 77, no. 3, p. 123s–132s, 1998.